Complex impedance spectroscopy for monitoring tissue responses to inserted neural implants

Justin C Williams[1]**, Joseph A Hippensteel**[1]**, John Dilgen**[2]**, William Shain**[2] **and Daryl R Kipke**[3]

[1] Department of Biomedical Engineering, University of Wisconsin-Madison, WI, USA
[2] Wadsworth Center, Albany, New York, USA
[3] Department of Biomedical Engineering, University of Michigan, MI, USA

E-mail: jwilliams@engr.wisc.edu

Abstract
A series of animal experiments was conducted to characterize changes in the complex impedance of chronically implanted electrodes in neural tissue. Consistent trends in impedance changes were observed across all animals, characterized as a general increase in the measured impedance magnitude at 1 kHz. Impedance changes reach a peak approximately 7 days post-implant. Reactive responses around individual electrodes were described using immuno- and histo-chemistry and confocal microscopy. These observations were compared to measured impedance changes. Several features of impedance changes were able to differentiate between confined and extensive histological reactions. In general, impedance magnitude at 1 kHz was significantly increased in extensive reactions, starting about 4 days post-implant. Electrodes with extensive reactions also displayed impedance spectra with a characteristic change at high frequencies. This change was manifested in the formation of a semi-circular arc in the Nyquist space, suggestive of increased cellular density in close proximity to the electrode site. These results suggest that changes in impedance spectra are directly influenced by cellular distributions around implanted electrodes over time and that impedance measurements may provide an online assessment of cellular reactions to implanted devices.

(Some figures in this article are in colour only in the electronic version)

Introduction

Microelectrode arrays can reliably record neural activity for several months in a high percentage of implanted animals (Liu *et al* 1999, Nicolelis *et al* 1997, Rousche and Normann 1998, Williams *et al* 1999a). While this is acceptable from many experimental standpoints, it is not acceptable for chronic clinical devices. In a truly effective neural implant, the working time span must be years instead of months with a large fraction of viable electrodes and stable extracellular recordings from day to day.

There are several underlying factors that may contribute to implant failure and the instability of extracellular unit recordings. Some portion of implant failure and variability may be attributed to reactive responses around the electrode implant sites (Edell *et al* 1992, Johnson *et al* 2005, Otto *et al* 2006). It is hypothesized that these reactions may alter the electrical properties of the surrounding tissue and even contribute to neuronal death (Agnew *et al* 1986, Grill and Mortimer 1994, Klein *et al* 1993).

There is considerable experimental evidence in the literature to support these arguments. The extracellular environment around implanted electrodes changes due to insertion-related damage and sustained responses promoted by the presence of a device in the brain (Turner *et al* 1999, Stensaas and Stensaas 1978, Szarowski *et al* 2003). Following electrode insertion, immediate vascular damage and brain cell damage can result in recruitment of cells from the peripheral

immune system as well as activation of resident microglia and astrocytes. These cellular events result in the development of a compact sheath of cells and accumulations of extracellular matrix material surrounding the implant (Spataro *et al* 2005). This tissue encapsulation can cause changes in the electrical properties of the tissue adjacent to an implant (Grill and Mortimer 1994, Xu *et al* 1997). This encapsulation tissue was found to have a higher resistance than normal tissue. Similar increases in tissue resistance have been observed following experimental ischemia and edema. These changes may be caused by decreases in the extracellular volume fraction (Klein *et al* 1993, Schuier and Hossmann 1980, Demirci *et al* 1997, Korf *et al* 1988). Similar changes in electrode performance have been observed in cell cultures, when cells in the local environment, or even in direct contact with an electrode, produce a change in electrode–tissue interface electrical properties (Giaver and Keese 1993, Ehret *et al* 1997, Kyle *et al* 1999, Buitenweg *et al* 1998, Merrill and Tresco 2005). These changes can affect the recorded signal from cultured neurons (Buitenweg *et al* 1998). Thus, changes in tissue electrical properties, e.g. impedance between device electrode(s) and a distant ground, may be used to assess tissue changes around inserted devices. We propose that these changes in electrical tissue properties will result in measurable changes in the impedance spectra measured using electrodes on implanted devices.

In order to test this hypothesis, we have investigated the relationship between impedance properties and histological reactions of implanted electrodes. Our results indicate that predictable relationships can be observed between impedance measurements and tissue reactions; thus changes in tissue impedance spectra may provide an on-line means to assess tissue–electrode interface properties.

Methods

Chronic recording arrays

Tungsten microwire electrode arrays were used in this study, the details of which can be found elsewhere (Williams *et al* 1999b). The tungsten microwires were constructed from a 35 μm tungsten wire with 7 μm polyimide coating. The individual microwires were fabricated into arrays with two rows of either eight or ten wires each (figure 1(A)).

Surgical procedure

Hooded Long Evan Rats weighing approximately 350 g were used in this study. Each rat was implanted with a single electrode array, implanted in the S1 cortical barrel region. Eleven animals were used resulting in 204 individual electrode recording sites (7 arrays consisted of 2 rows of 10 electrodes and 4 arrays consisted of 2 rows of 8 electrodes). Surgical implantation of the arrays followed standard published procedures (Williams *et al* 1999b, Rousche *et al* 2001). Briefly, the animals were anesthetized and the scalp and muscle above the intended implant site were reflected. A small craniotomy hole (∼1.5 mm) was made in the skull. The dura mater was reflected and the electrode was

inserted through the pia mater. The craniotomy was filled with gelfoam and a connector was secured with dental acrylic. The remaining exposed skull and electrode interconnects were covered with dental acrylic. The skin was sewn around the acrylic cap and connector.

Impedance testing procedure

Prior to implantation, each electrode was tested in physiological saline and sterilized in ethylene oxide gas. Complex impedance spectra were measured using an HP4284 LCR meter in a constant voltage mode, with the electrode (two-electrode method) referenced to a distant low impedance stainless steel (316SS) ground screw (ANSI #2–56, nominal diameter ∼2 mm). The two-electrode method is suitable for measuring impedance from microelectrodes due to the large difference in impedance relative to the reference and the small current that passes through the circuit (Brett and Brett 1993). While measuring the impedance properties, it is important to use a constant potential method such that changes in electrode properties due to the changing electrode potential are not misinterpreted (Weiland and Anderson 2000). A constant voltage of 5 mV was used, producing a nominal current of less than 50 nA at 1 kHz. The complex impedance was measured using a sinusoidal input voltage over a range of frequencies from 100 Hz to 2 kHz sampled at 100 Hz increments. Complex impedance values were plotted versus frequency to allow for qualitative comparisons with the published literature (figure 1(B)). To aid in interpretation of the relative changes in the real and imaginary impedance components, the complex impedance was presented as Nyquist plots, where the resistance versus the reactance for each frequency was plotted (figure 1(B)).

After implantation, the impedance spectra were measured for each electrode using the same protocol used during the saline test. This process was repeated 20 times daily to establish the statistical distribution of variability in the measurements. Electrodes were again tested in physiological saline after explant to measure any potential change in the fundamental electrode electrical properties.

Histological techniques

The implanted animals in this study were divided into two groups, based upon implant duration with survival times of 7 or 21 days. These time periods were chosen to correspond to different phases of brain reactive responses (Turner *et al* 1999, Szarowski *et al* 2003, Polikov *et al* 2005, Kim *et al* 2004). At the end of the implant duration, animals were tested with the impedance protocol to obtain an endpoint measurement and were then immediately terminated and prepared for histological evaluation. Animals were perfused with phosphate buffered saline (PBS) through a cannula that was inserted into the left ventricle and fed up through the ascending aorta. This was immediately followed with 4% paraformaldehyde for tissue preservation. The skull was then stored in fixative for an additional 24 h. Care was taken to avoid contact of the connector with the fixation fluid, as this may have precluded post-explant impedance
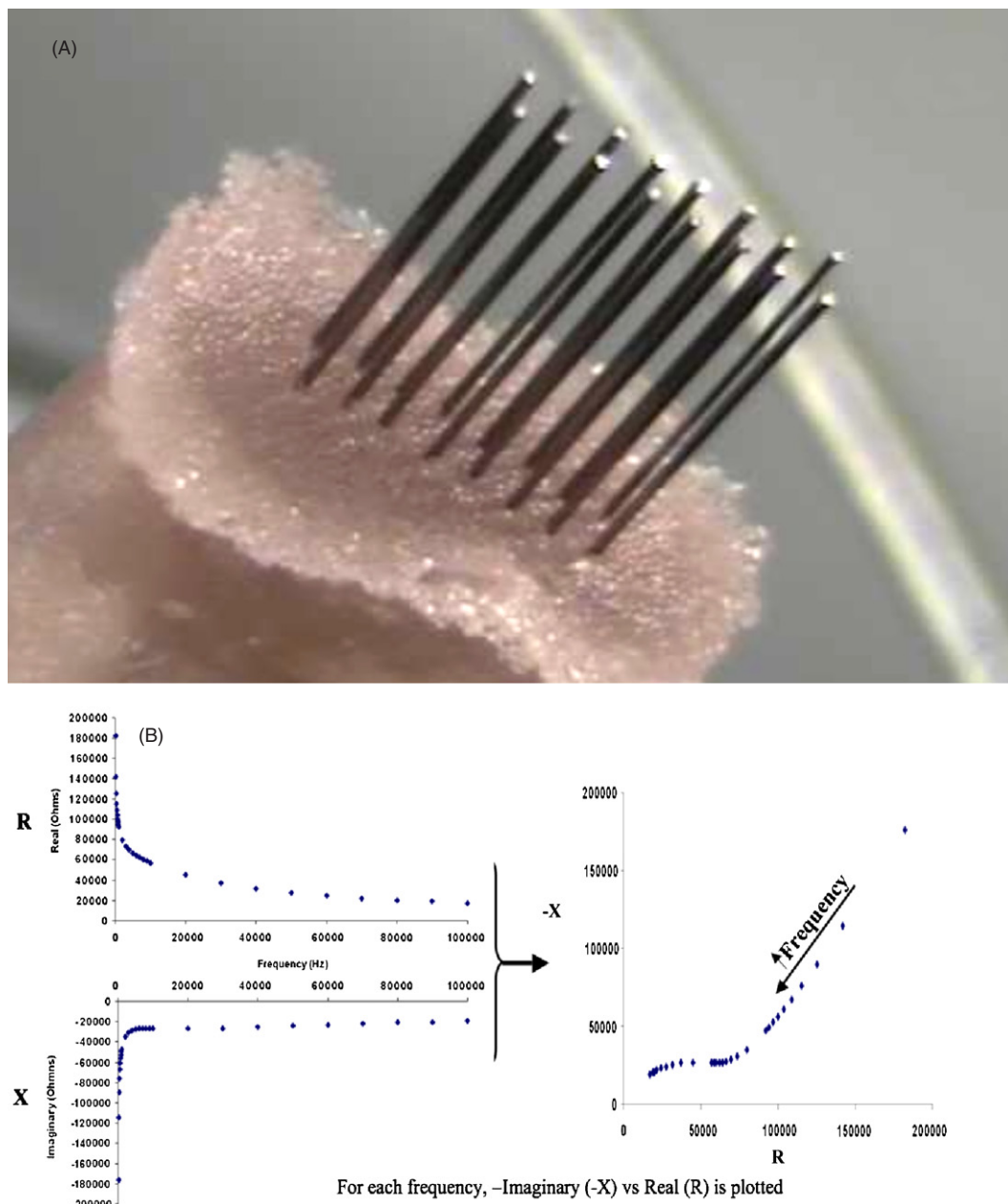
Figure 1. (A) Micrograph of a typical implanted electrode array consisting of two rows of eight tungsten wires. (B) General procedure for forming Nyquist plots from complex impedance spectra.

testing. Subsequently, the device was withdrawn and stored for separate analysis. The entire device was first imaged at low magnification and the individual wires were then removed for high magnification imaging. The brain was then removed from the skull and blocked for additional processing. The blocked brain samples were oriented to permit vibratome sectioning of 100 μm thick tissue slices perpendicular to the trajectory of inserted microwires (see figure 2).

Tissue slices were stained using standard immunohistochemistry protocols (Turner *et al* 1999, Szarowski *et al* 2003, Spataro *et al* 2005). Prepared tissue slices and wires were separately mounted between coverslips in a glycerol solution saturated with n-propyl gallate to reduce photobleaching. In this way, imaging can be made from either side of the sample insuring that we can image through the entire thickness of each tissue slice. Samples were viewed using an Olympus IX70 inverted fluorescence microscope. Data collection conditions were established for tissue samples from each immunohistochemistry run so that changes in color intensities in the final images reflect changes in fluorescence intensities. A NORAN Instruments confocal laser scanning attachment was used to collect 3D sets that represent the entire thickness of each tissue slice. Data was collected using
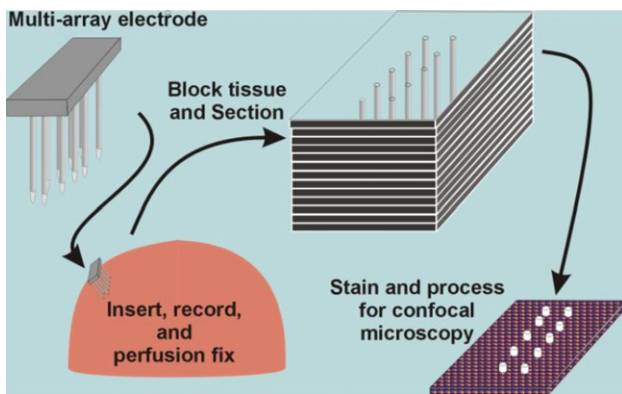
Figure 2. Schematic representation of the histology protocol. After the experimental procedure is completed, the tissue is perfusion fixed and the electrode is removed. The tissue is then sliced perpendicular to the electrode tracts in 100 μm sections. The sections are then stained and imaged with confocal microscopy.

either a 10 × (0.40 N.A.) or 40 × (1.15 N.A.) objective lens. Images were typically presented as through-focus *X, Y* projections (Intervision Software, NORAN).

Data collection was made in a multi-step process. First, lower magnification images were collected and a composite image prepared using a tissue slice from approximately halfway down the length of a wire, assuming that these were inserted perpendicular to the brain surface and that they traveled in a straight line. These composite images were used for the identification of as many of the traces left by the wires as possible and to establish fiduciary landmarks, e.g. major blood vessels, that would permit data collection of the same region in a series of adjacent tissue slices that began at this point and extended beyond the tip of the longest traces. Wires frequently did not travel in the anticipated trajectories. For final analysis, a series of overlapping higher magnification images were collected from each tissue slice so that the entire field of traces could be observed. Tissue slices were typically examined from the midpoint down the longest trace to the tissue slice beyond the tip of the longest trace. This strategy provided multiple observations of the trace of each wire, thus ensuring a high level of confidence that each trace was properly identified. It also allowed us to recognize the tip of each wire. Representative data are presented.

The raw data from the confocal microscope were colorized and adjusted using Silicon Graphics Intervision software in order to maximize the quality of all images. All data sets were modified in exactly the same manner, so the results could be compared across all of the data. In the images presented here, astrocytes were labeled with primary antibodies to glial fibrillary acidic protein (GFAP) (Amat *et al* 1996) and visualized using a Texas Red-labeled secondary antibody, vascular endothelial cells were labeled with antibodies to glucose-transporter-1 (GLUT-1) (Mooradian 1997, Loda 2000) and visualized using an Alexa488-labeled secondary antibody, and nuclei were labeled with DAPI (4′, 6-diamidino-2-phenylindole). The images were prepared using false colors: red for astrocytes, blue for GLUT-1 and green for DAPI.

Results

For clarity and consistency, data from a single, representative animal will be described and analyzed in detail. This allows for a coherent analytical progression to develop a clear correlation between electrode tract histology and complex impedance. These results are supplemented by summary data to extend our conclusions beyond this single animal. This particular animal was chosen due to the presence of a variety of histological responses within a single electrode array.

Impedance measurements

Impedance measurements were first made in saline to provide a baseline of electrode characteristics. Impedance spectra were measured as real and imaginary pairs. Impedance magnitude and phase were computed and plotted to facilitate a preliminary qualitative comparison of the data with the published literature. The complex impedance spectra measured on electrodes in saline exhibit impedance decreases with frequency. The impedance in saline was nominally 25 kΩ at 1 kHz. The corresponding phase plot (not included) showed a phase angle near 45°, typical of many types of solid metal electrodes (McAdams *et al* 1995). These preliminary saline recordings were used to assure efficacy of the recording device. Nyquist plots were used to describe impedance changes over the entire range of measurements (figure 3). The impedance loci were strongly clustered, exhibiting low variability in the real or imaginary components. The loci were also all very linear in their *R–X* relationship, typical of what would be seen of a metal electrode in saline (McAdams *et al* 1995).

Impedance measurements from electrodes chronically implanted in the brain were different from those observed following initial insertion (figure 3). A representative data set for one electrode has been plotted to illustrate the real (figure 3(A)) and imaginary (figure 3(B)) components, both immediately after insertion and 7 days after implantation. While qualitatively the general shapes of the *R* and *X* plots look similar across the plots, they are generally increased, resulting in an impedance magnitude of 140 kΩ at 1 kHz. The Nyquist plots of 20 electrodes on day 7 demonstrated that the electrodes in the array appear to have a substantially higher real component and no longer exhibit a linear relationship between *R* and −*X* (figure 3(D)). A number of the electrodes in this array exhibited a nonlinear behavior, and had a large variability in the imaginary component of the impedance spectra, particularly at high frequencies. The nonlinearity manifests itself in the form of a semi-circular arc at high frequencies and an increased curvature across all frequencies, the former being indicative of a classical parallel RC (resistive/capacitive) component. This is a trend seen throughout our results and will henceforth be referred to as an RC effect. These aspects are similarly observed in the impedance spectra reported using other types of electrode arrays (Johnson *et al* 2005).

General impedance trends

In traditional neurophysiology experiments, magnitude impedance is generally measured at 1 kHz to test for electrode
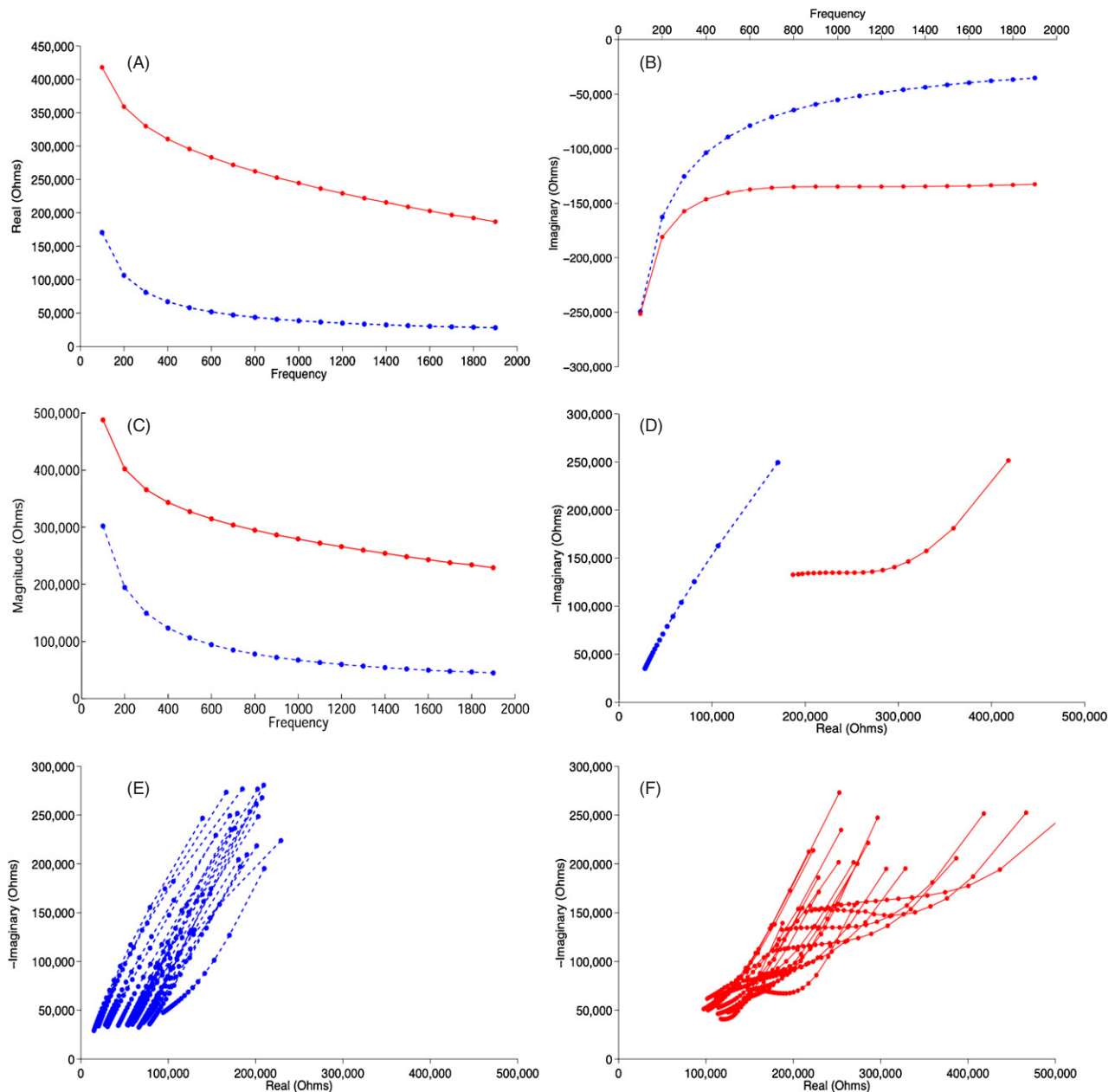
Figure 3. Complex impedance spectra from a single electrode taken immediately following implantation (dashed/blue) and 7 days post-implant (solid/red). (A) Real component, (B) imaginary component, (C) standard Bode plot and (D) Nyquist plot ordered complex pairs (R versus $-X$) at each frequency. Nyquist plots for 20 electrodes immediately after implantation (E) and after 7 days (F).

patency. In fact, most experimental and clinical impedance measuring devices are set to only measure the impedance magnitude at 1 kHz. As a first step in analyzing the changes in electrode impedance seen after implantation, the 1 kHz impedance properties were plotted over a 19 day period following insertion (figure 4).

When impedance measurements across a single array at 1 kHz were observed over the first 7 days post-implant, a trend for increasing average impedance was observed (figure 4). For this particular implant, R, X and Z all increased monotonically over the first 7 days, with a corresponding increase in the

variation across the array on subsequent days. The phase value (theta, not shown) increased over the first 5 days before reaching a steady state. In all cases the variation of values about the mean was relatively large across the array, suggesting some independence in the measurements from one electrode to another.

Across all animals, the general trends shown in figure 4 were seen over a 19 day period. A plateau in impedance measures was observed from days 7–10, with a subsequent drop off to asymptotic values observed at longer times. The 1 kHz magnitude impedance (Z) increases from a range of
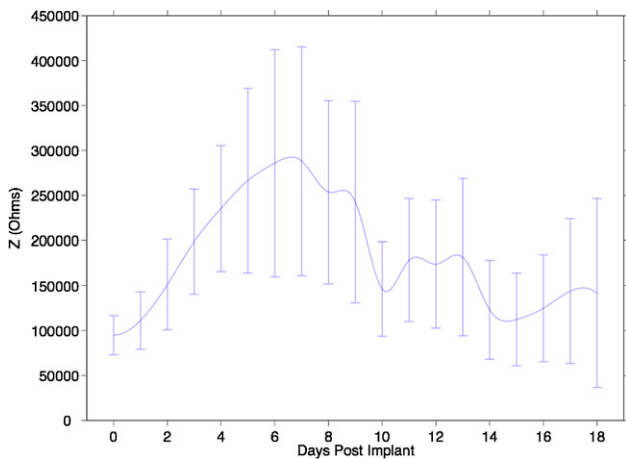
Figure 4. Magnitude impedance (Z), measured at 1 kHz over an 18-day period post-implant. The solid line shows the mean of all of the electrodes and the error bars signify the standard deviation. This data is from 80 individual electrode sites (spanning four animals), each measured 20 times daily.

75–125 kΩ on the first day to a range of 200–375 kΩ on day 7. The 1 kHz impedance phase angle (not shown) increased from an average of approximately 50° on the first day to approximately 60° between days 5 and 8, although the range of values for theta varies widely from day to day.

Histological results

Immunohistochemistry was used to describe reactive responses around all wires of inserted devices. Thick tissue slices were prepared and imaged to describe responses along wire tracks including the tips. A representative composite image prepared from one tissue slice along the length of wires demonstrates our abilities to recognize and identify electrode

tracks (figure 5). The locations of the wire tracks were identified using higher magnification images. One row of wires (1–10) showed significant displacement. Wire 1 was on nearly the same line as wires 5–8 and 10, but appears displaced along the long axis of the device. Wires 2–4 and 9 were displaced laterally. While the other wires were arranged linearly, a space between wires 5 and 6 exists suggesting that these wires were also displaced along the long axis of the device.

Reactive cell responses are indicated by increased GFAP (red) labeling (Turner *et al* 1999, Szarowski *et al* 2003, Kim *et al* 2004, Polikov *et al* 2005). The large acellular region that was labeled nonspecifically by the secondary antibody used for visualizing anti-GLUT-1 depicts a large lesion probably produced by severing a larger blood vessel. Wire tracks were evaluated by evaluators blind to the impedance analysis and classified as being either associated with more reactive responses, e.g. increased GFAP labeling or the large acellular lesion (orange dots), or associated with healthier tissue (yellow dots); only tracks 9 and 10 were not associated with either increased GFAP labeling (tracks 1–4 and 8) or the acellular lesion (wires 4–7). In the other row, only tracks 14 and 15 were associated with increased pathology, while the remaining tracks 11–13 and 16–20 were associated with less reactive, healthier tissue.

Correlation of impedance trends and histology

In order to correlate the histological findings with impedance spectra, results obtained from the histology were compared to complex impedance spectra recorded just prior to brain perfusion on day 7 (figure 6(A)). The 20 traces of figure 6(A) correspond to each electrode in the array. Each trace represents the Nyquist plot of the complex impedance spectrum for each day. The spectrum for each electrode was placed into one
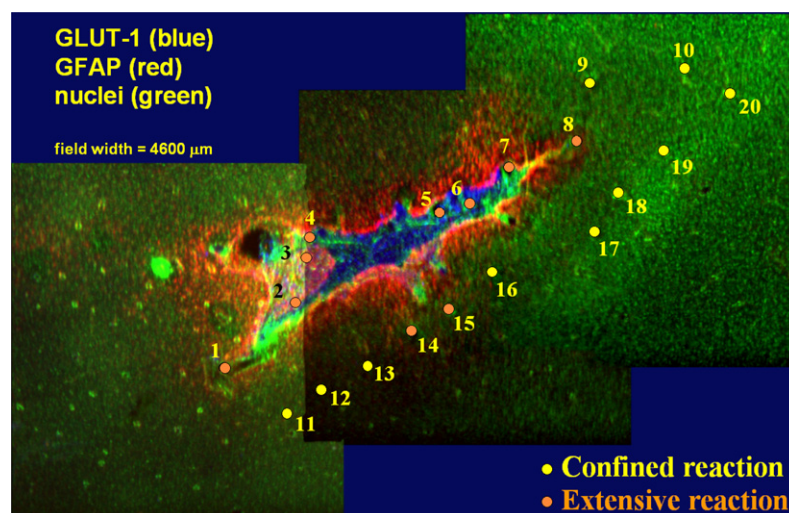

Figure 5. A composite confocal image of tissue around an implanted electrode array. The tissue is triple stained with GLUT-1, GFAP and DAPI to stain for blood vessels, astrocytes and cell nuclei, respectively. The electrode sites are indicated by the numbered circles, with the yellow circles denoting confined reaction regions and orange dots denoting extensive reactions.
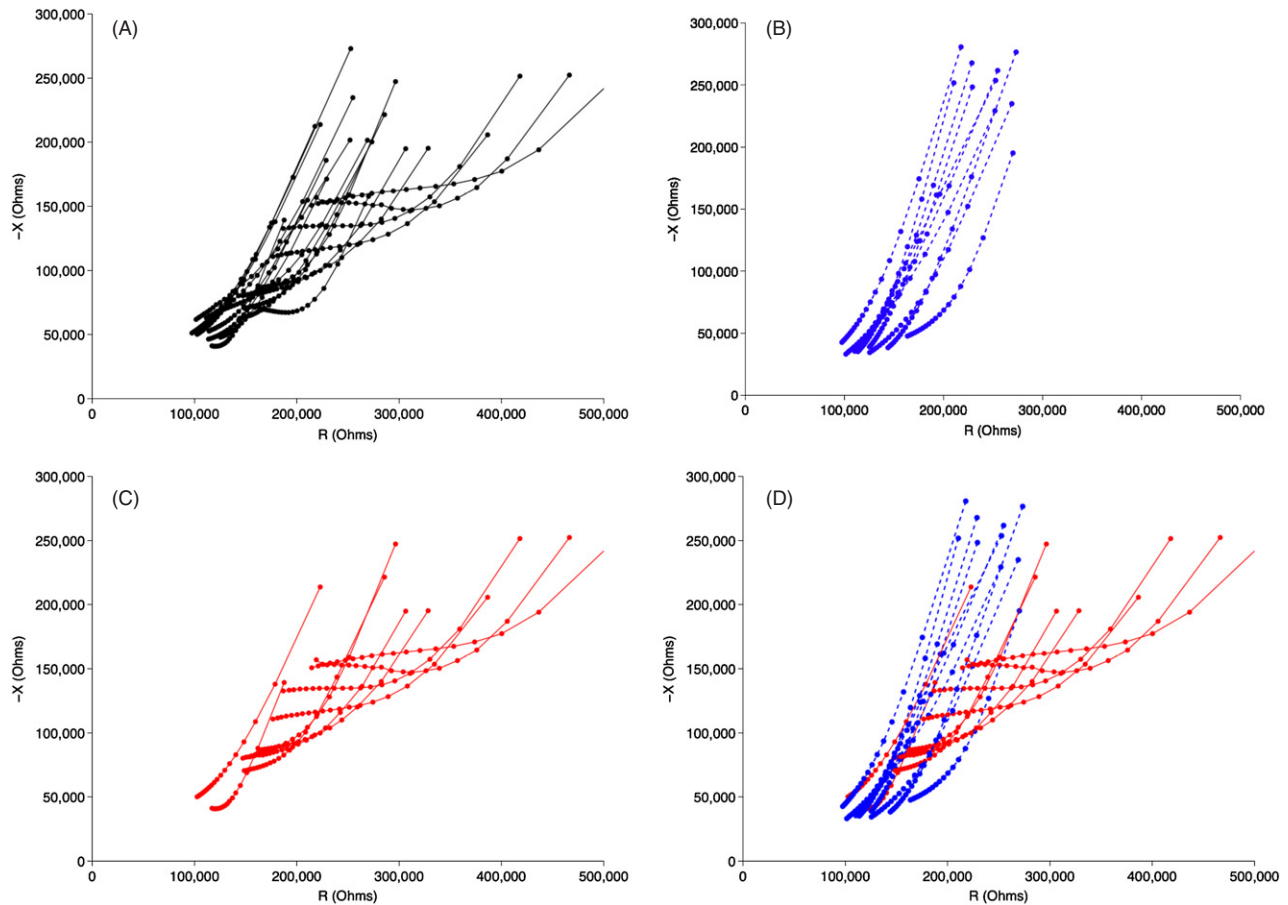
Figure 6. Nyquist plots for 20 electrodes grouped by histological reaction, 7 days post-implant. (A) All electrodes plotted together. (B) Electrode sites exhibiting a confined histological reaction. (C) Electrode sites exhibiting an extensive histological reaction. (D) All electrodes color coded by reaction level (solid/red = extensive reaction, dashed/blue = confined reaction).

of two groups based on the histological reactions observed (figure 5), color coded and plotted separately (figures 6(B) and 6(C)) and then again together (figure 6(D)). Several spectral features distinguished the two groups. There was an overall lower R component in the electrodes associated with tracks having reduced reactive responses (blue group), especially at low frequencies, and an R versus $-X$ relationship including a marked RC effect in the electrodes associated with tracks with larger reactive responses (red group) resulting in higher X components at higher frequencies. Although many of the correlations followed this pattern, several exceptions were observed. One electrode assigned to the blue group had a trace with an apparent RC effect, and two fairly linear traces were observed in the red group. These three examples may represent misclassification of tracks using histological analysis, which can be complicated due to the resolution, qualitative nature of this assessment, improper identification of the electrode tip or damage to the electrodes.

The impedance spectra from the same implant on the first 6 days post-implant were grouped as presented in figure 6, to observe how the two groups of impedance measurements evolve over time (figure 7).

Figure 7 shows complex impedance spectra for all 20 electrodes from the array on four individual days post-implant. The color of each trace corresponds to the group that the individual electrode was assigned, based on histology. In the day 0 plot, all the electrodes displayed a linear R versus $-X$ relationship, similar to that seen with the electrode in saline. No apparent differences between the distributions of the red and blue plots were observed at this time. In the day 2 plot, the majority of the traces continued to exhibit a linear R versus $-X$ relationship and the two groups continued to be randomly distributed. In the day 4 plot, a number of traces started to exhibit an R versus $-X$ relationship with a high frequency RC arc, although the distribution was not well defined. In the day 6 plot a number of electrode traces exhibited an R versus $-X$ relationship with a large RC arc component, the majority coming from the 'extensive' reaction group, shown in red. The figure illustrates that the distribution of the two groups evolved over time, becoming well established somewhere between days 4 and 6, and was not a result of an initial grouping of the electrodes due to some intrinsic difference in electrode properties or initial differences in tissue properties around individual electrodes or groups of electrodes. While these groups appear to develop over time, it is not clear whether
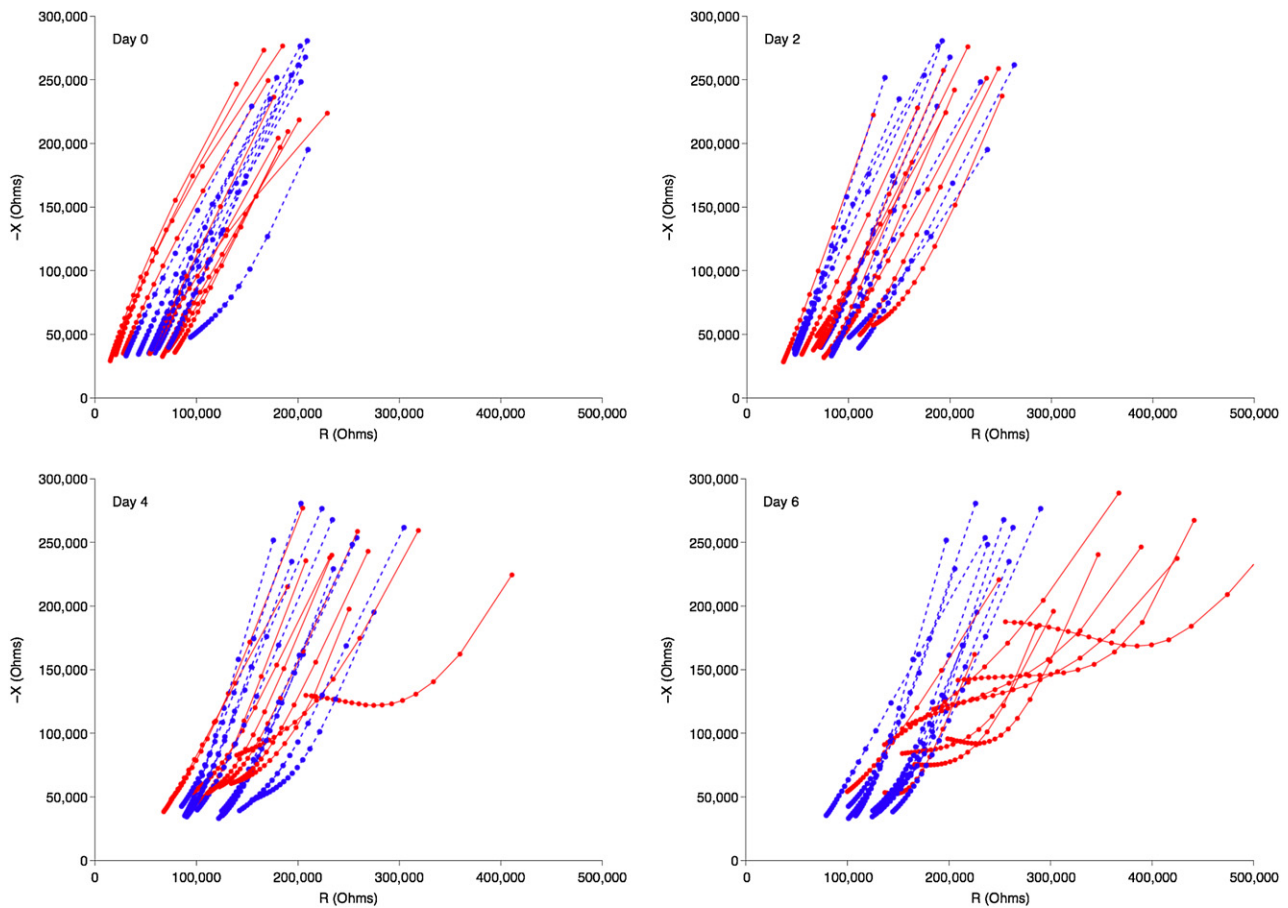
Figure 7. Nyquist plots for 20 electrodes, grouped by histological reaction (solid/red = extensive reaction, dashed/blue = confined reaction)., over subsequent days post implant; (A) Immediately post implant. (B) 2 days post implant. (C) 4 days post implant. (D) 6 days post implant.

these trends are a result of systematic changes in individual electrodes or randomly distributed changes within the two groups.

To gain some insight into this issue, two electrodes were chosen from the impedance data in figure 6 to describe the overall trends seen in the entire array. Representative electrodes were chosen from the 'confined' (figure 8(A)) and 'extensive' (figure 8(B)) reaction groups. The impedance loci for each electrode were plotted simultaneously for every day of the implant. The electrode in figure 8(A) exhibited low impedance variance over time when compared to an entire array. The impedance loci exhibited a noticeable RC effect at high frequencies. The electrode in figure 8(B) exhibited a large increase in the real component of the impedance at low frequencies and a large increase in the imaginary component at higher frequencies. This resulted in an increased RC arc over almost the entire frequency range by the final day of the implant. This trend also seemed to develop gradually over the duration of the implant, becoming more pronounced with each consecutive day. It is notable that this change occurred gradually, and systematically, without any noticeable jumps or irregularities from one day to the next.

Summary of implant results

The results to this point have focused on the impedance and histology from the electrodes from a representative implant. The results have been presented in this manner to preserve continuity in the progression of data analysis and histological correlations. Also, this reduces any complexity produced by between-subject variability. For the results to be compelling, it is necessary that they generalize to multiple implants. From the implants used in this study, a total of 44 of the implanted electrode sites were successfully recovered, imaged and analyzed. The remaining implants either came from animals that did not perfuse adequately (three animals), had surrounding tissue destroyed during explant (one animal), did not label properly (one animal) or were improperly sectioned for identification of individual electrode tracts (two animals). From the remaining four animals, 44 out of the 68 implanted electrode sites could be positively identified in the histology images. For all the implants, individual electrode implant sites were excluded from analysis if they could not be accurately matched to a corresponding electrode in the array.

The recovered electrode sites from all the implants were divided into two groups representing extensive reactions
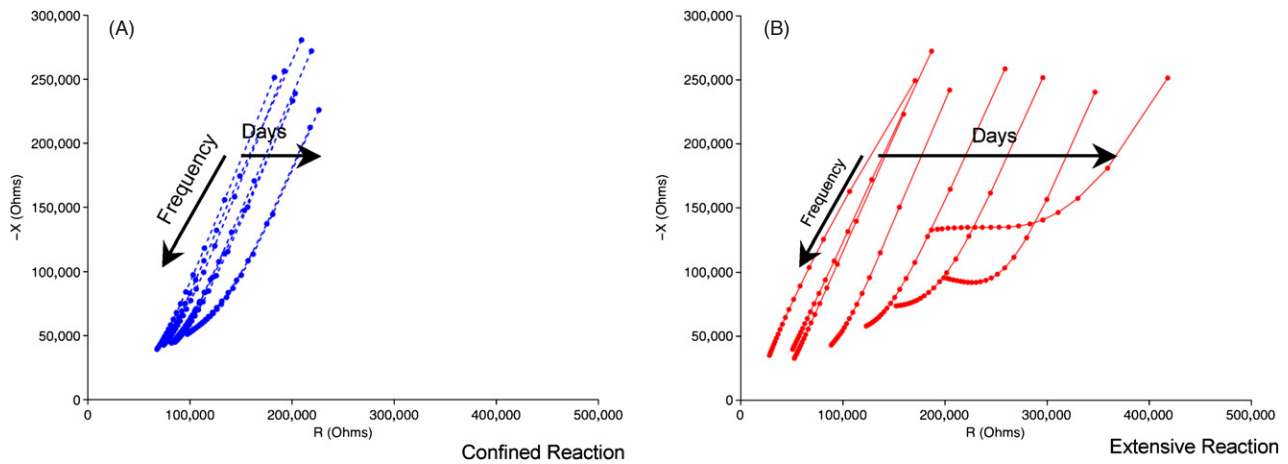
417

Figure 8. Nyquist plots for two different electrodes, one characterized as having (A) a confined reaction and (B) an extensive reaction. For each plot, data are presented immediately following implant and on each of the first 7 days post-implant.
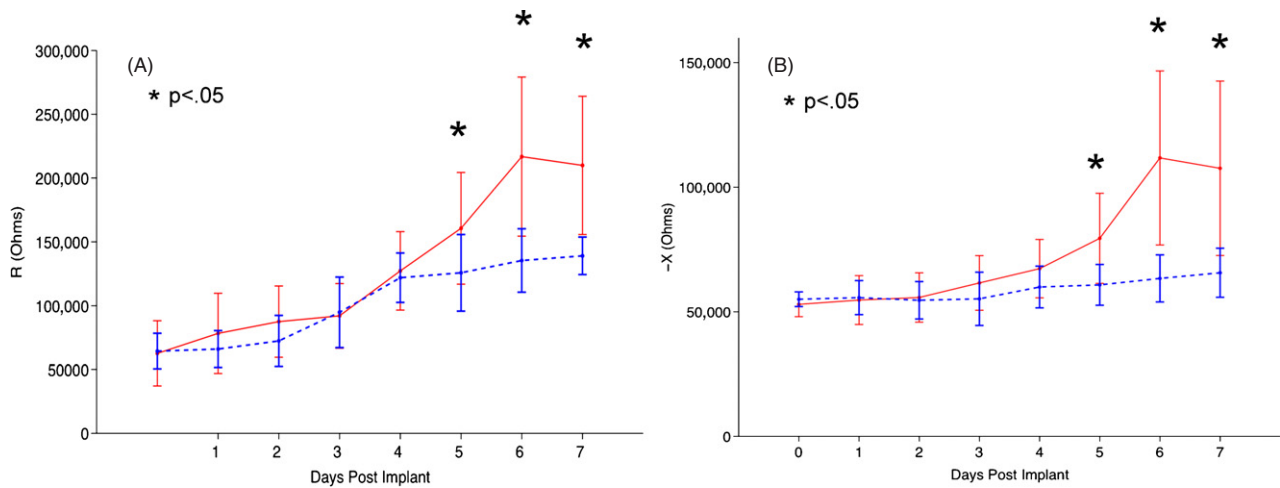

Figure 9. Average complex impedance values over time: (A) real component of impedance (R) and (B) imaginary component (X). The solid (red) line is for the electrodes with an extensive reaction ($n = 10$) and the dotted (blue) line is for the electrodes with a confined reaction ($n = 10$). The error bars in both cases are the standard deviations. The asterisks denote days when the two electrode groups were significantly different ($p < 0.05$)

(Group E) and confined reactions (Group C). All of the histologically identified implant sites were from the 7-day implant time period. Figure 9 shows the 1 kHz impedance trends for these two groups. Both groups start out at similar levels, for both the real and imaginary impedance components. In these plots, both the real and imaginary components of the impedance for these electrodes started to diverge on the fourth day. The extensive reaction electrode values climbed to significantly higher levels in both plots, even though the electrodes from the confined group starts at a higher initial impedance. Also notable was that the variability in the daily measurement values (as indicated by the standard deviation) also increased as the impedance values increased in the extensive reaction electrode. These plots showed a trend of increasing resistance and reactance over time, with statistically higher impedances on electrodes with extensive reactive responses. For all of the electrodes ($n = 44$) on days 5, 6 and 7, the differences between the two groups were

significantly different (power >0.9, $p < 0.05$). Although these trends were significant, they still highly depended on the initial individual electrode impedance values and made it difficult to identify reactive responses merely by looking at the magnitude impedance at 1 kHz without prior knowledge of the overall time-variant trends. From figure 8, there appeared to be features in the impedance spectra that may be more informative of the level of reactive responses.

To further illustrate the effects of reactive responses on individual electrode impedances, we examine another electrode array that had highly variable reactive responses. Figure 10 shows the results from another implanted electrode array, which exhibited a progressive reactive response across one row of the electrode, being confined at one end of the array and progressing toward a very extensive reaction on the other end. The plot in figure 10(A) shows the impedance loci of three of the electrodes in a single row of the array (representing one electrode from the proximal end, the middle
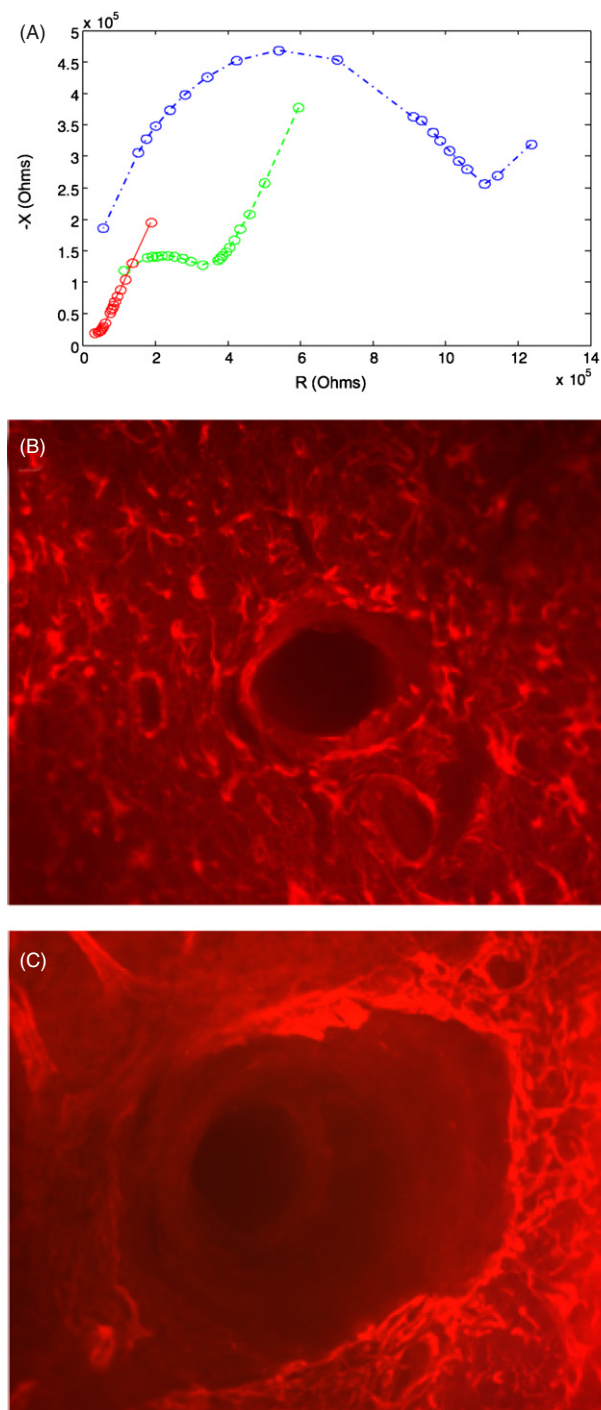
Figure 10. (A) Nyquist plots for three electrodes in a single row of an electrode array and the corresponding tissue around two individual electrodes. (B) GFAP-stained tissue section around the electrode denoted by the solid (red) line in A. (C) GFAP-stained tissue section around the electrode denoted by the dashed (green) line in A. The dotted-dashed (blue) line in (A) is the impedance spectra from another electrode that had a significant extensive reaction (not shown), resulting in a tissue void several times larger than in image (C).

and the distal end of the array), immediately prior to sacrifice on the seventh day of the implant. The solid (red) and dashed

(green) traces highlight the impedance locus of the electrode tracts that were shown in the histological images (figures 10(B) and 10(C)). It can be seen that this implant qualitatively followed the results seen from the previous array (figures 5 and 6). The confined reaction in figure 10(B) corresponded to a linear impedance locus relationship (solid/red trace in figure 10(A)) and the extensive reaction in figure 10(C) corresponded to an impedance locus with a clear RC arc at high frequencies (dashed/green trace in figure 10(A)). It should be noted that the image in figure 10(C) shows part of a large void, several times larger than the expected electrode tract, surrounded by dense GFAP positive cell sheath. The void was produced by a sheath of dense GFAP positive cells that remained attached to the shaft of the electrode and came out when the implant was explanted (not shown). Also notable is that the impedance loci with the largest impedance value and most apparent RC effect in figure 10(A) (dotted-dashed/blue line) also had a very extensive histological reaction. A similar void (not shown) was produced around that electrode tract as to that in figure 10(C), but many times larger in diameter. This void was also produced by a very dense sheath of GFAP positive cells that remained tightly attached to the electrode shaft when the array was explanted. In general, the presence of increasingly larger reactive responses results in an overall increase in both real and imaginary impedance values, but more importantly results in the formation of the aforementioned RC effect manifested as a semi-circular arc in the spectrum at high frequencies that becomes highly prominent in very extensive reactive responses.

Discussion

Results from this study characterize changes in the complex impedance spectra of implantable microelectrodes over time. The observed changes in impedance spectra are consistent with the expected time course of biological reactions to implanted devices (Turner *et al* 1999, Szarowski *et al* 2003). The results of the study also show that differences in impedance spectra are spatially distributed within an electrode array. This suggests that some component of impedance changes is caused by factors that are locally isolated to individual electrodes or groups of electrodes rather than factors related to the implant as a whole. This is consistent with studies describing immune reactions to electrode arrays in which individual electrodes within an array elicit immune responses independent of adjacent electrodes (Rousche and Normann 1998, McCreery *et al* 2000). This motivates the current study's goal: to correlate impedance changes with reactive cell responses observed around individual electrodes. The microwire types of implants used in this study are particularly useful because they are spaced far enough apart that independent discernable reactions can be seen at individual sites in the array. Also, there are multiple sites (20) within a single implant so that a greater variability is seen across the array and a large sample size can be obtained from an individual animal.

The goal of this study was to associate reactive responses with impedance changes. Our analysis allowed us to describe clear regions of extensive reactive responses around

each electrode track, making it possible to classify reactive responses as 'confined' or 'extensive'. It is not uncommon to observe a wide range of histological reactions to individual electrodes in a chronically implanted microelectrode array (Rousche and Normann 1998, McCreery *et al* 2000). If the histology differences seen in our two groups were not large enough and did not correlate with detectable impedance changes, then impedance measurements would not have the potential to discriminate more subtle differences in histologically described reactive responses.

Traditionally electrode impedance has been measured to test for patency of the electrode insulation after implantation. This was done by measuring the magnitude and phase at a single frequency. This frequency was usually picked to be 1 kHz, mainly because this is the fundamental frequency of a neuronal action potential, which has a time period of approximately 1 ms. It was thought that this would be the frequency component of the electrode impedance that would primarily affect the recorded signal from surrounding neurons. Due to the fact that most traditional neurophysiology electrode impedance monitoring equipment is set up to measure the impedance magnitude at 1 kHz only, it would be useful to be able to correlate 1 kHz impedance to the tissue state around an implanted electrode.

The initial results presented in this study suggest that large differences in cell reactive responses result in larger impedance values at 1 kHz. This helps to explain some of the variance in the overall impedance trends seen in figure 4. While there is a clear trend in figure 4 over time, there is a large variance on individual days. This is consistent with the idea that this data actually represent the combined data from at least two populations (confined and reactive) that each has its own population mean. The data in figure 4 are the addition of a population that has a low mean and small day-to-day changes (the confined reaction group) and a population that has a higher mean and larger day-to-day changes (the extensive reaction group). By adding these two groups together, a trend that follows the reactive response would still emerge, but its variance on individual days would be large. It is not known how sensitive this measure will be and whether changes at other frequencies may be more indicative of more subtle variations in histological reactions and local cellular densities. To address these issues, we have developed methods to produce *in vitro* tissue constructs where cell numbers, types and densities may be controlled (see Frampton *et al* 2007).

In the complex impedance loci in figure 8, it can be observed that there are features that distinguish the two groups from one another, an overall lower R component in the blue group, especially at low frequencies, and a curved R versus $-X$ relationship including an RC effect in the red group that results in a higher X component in that group at higher frequencies. Although this is generally the rule, several exceptions can be observed: one trace including a distinct RC effect in the blue group and two fairly linear traces in the red group. This is likely due to the subjective nature of the histological reaction grouping, which can be complicated by an inexact location of electrode sites. However, a clear qualitative correlation can be made between the extent of

reactive responses and impedance spectra features. As can be seen in figure 10, a progressive relationship can be seen between increasing reactive responses and the development of an RC effect in the Nyquist plot. This result is consistent with our model of impedance spectroscopy. As current leaves the electrode and enters the tissue compartment, it can be conducted along two pathways, either around and between cells (a resistive pathway) or through and across cells (a capacitive pathway). As current spreads away from the electrode and through the tissue, at any point in space it may be traveling in one of these two pathways (figure 11(C)). This results in a distributed network of parallel resistive and capacitive pathways, which from the impedance measurement system appear to be a lumped parallel RC network. At low cell densities, there are sufficient numbers of low resistance pathways for current flow to follow, such that the capacitance contribution is masked. As the cell density increases, the extracellular space decreases, thus reducing the low resistance pathways and causing current flow through cellular, e.g. capacitive, compartments. Also, the impact of the surrounding tissue on the impedance measurement is heavily influenced by the volume immediately surrounding the electrode, as the voltage drops off in all directions as it spreads through the tissue volume to the ground. Therefore, the influence of reactive cells will have a more significant effect as the cell density immediately adjacent to the electrode surface increases. Our data support this theory since the time course of impedance correlates with the expected time course of reactive responses (figures 4, 7 and 8, and Szarowski *et al* 2003), and that clear impedance spectral signatures arise in cases where there is significant accumulation of dense reactive cells in the immediate volume adjacent to the electrode (figure 10). Qualitatively, the impedance spectral signatures match those reported for chronic implantation of other types of electrodes (Johnson *et al* 2005). Although no histology was reported in that study, it suggests that the phenomena and relationships reported here will be extendable to other types of electrodes. To better understand the effects of spatio-temporal cellular distributions on impedance measurements also requires an experimental system where some of these factors can be systematically studied. We have started to explore this with a 3D tissue culture model of astrocyte–device interactions (Frampton *et al* 2007). We have started to develop a lumped parameter model (Johnson *et al* 2004, Otto *et al* 2006) to better interpret the theoretical effects of these different current-carrying pathways on measured impedance spectra. Additionally, the model can be used to account for differences in the initial electrode impedance for different electrode types and sizes.

The above lumped parameter model was largely guided by similar efforts to relate impedance spectroscopy results to physical correlates *in vitro* (Buitenweg *et al* 1998, Kyle *et al* 1999). Our approach is a three-component model consisting of an electrode–tissue interface, an encapsulation region and a neural tissue component. This electrical model and its physical interpretation are illustrated schematically in figures 11(A) and 11(B), respectively. Due to the commutative property of electrical components in series,
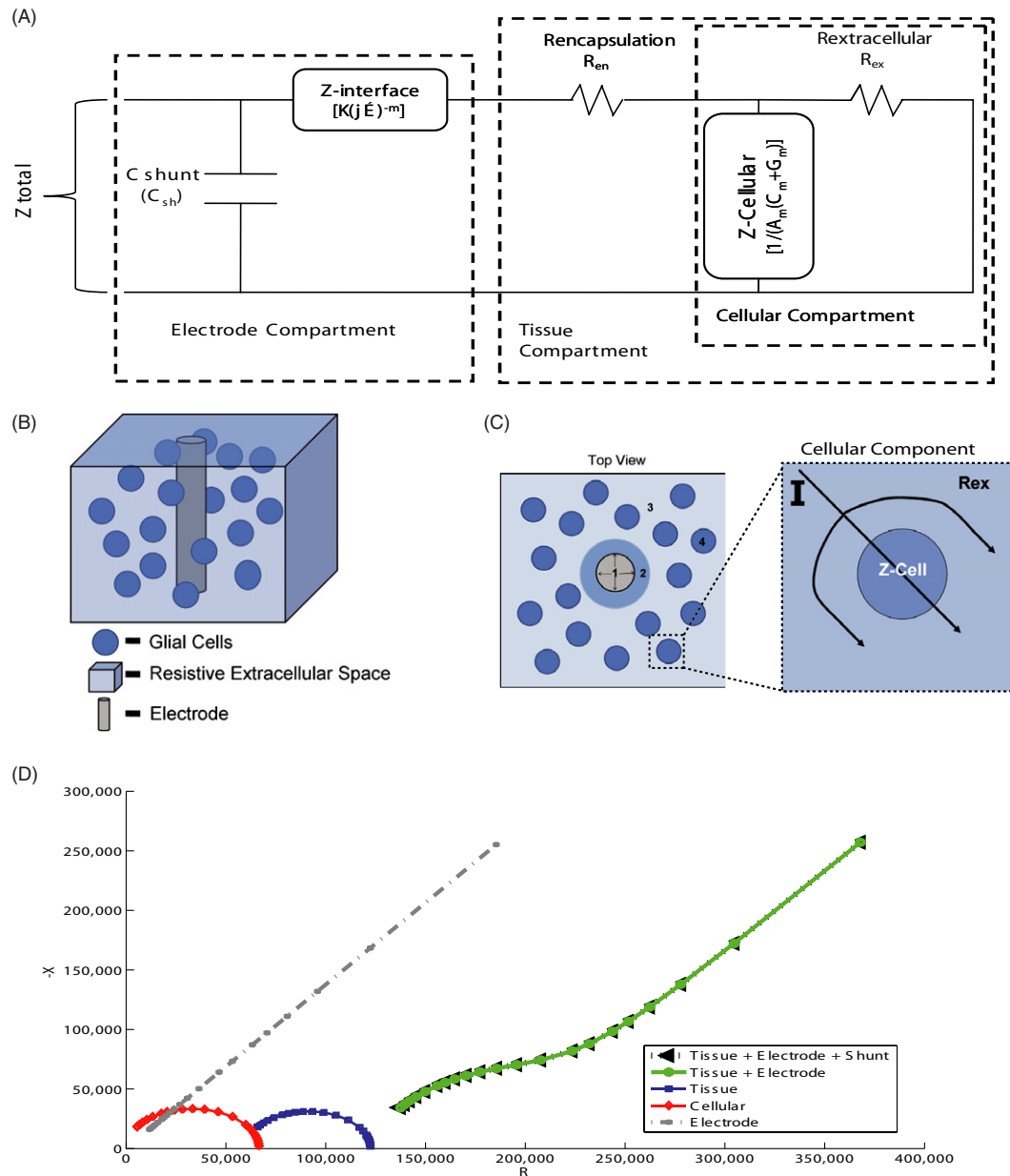
Figure 11. Model circuit diagram and physical interpretation. (A) Lumped parameter circuit model developed to delineate the impedance variation commonly found during *in vivo* impedance spectroscopy. (B) and (C) Three-dimensional and two-dimensional rendering of theorized physical components of the model. (C): 1 depicts the electrode–electrolyte interface, 2 is the protein-rich encapsulation layer (R_{en}), 3 represents the resistive extracellular space found between individual cells (R_{ex}) and 4 refers to glial cells (g_m and C_m, scaled by A_m). The right side illustrates the concept of current flow through the tissue component of the model, choosing passage either through the cellular component or resistive extracellular component, R_{ex}. (D) Nyquist representation of expected model results from a typical *in vivo* impedance spectrum (100 Hz to 10 kHz).

models based upon impedance measurements cannot be used to explicitly determine spatial distribution; although when paired with histological observations, spatial distributions of model components may be inferred. A description of this model following the path of a stimulus from a recording site to ground is provided.

The electrode–tissue interface of this model has been well established and consists of a constant phase element (CPE) wholly described by two coefficients: *K* and *m* (McAdams *et al* 1995, MacDonald 1992). This element takes the theoretical form of $K(j\omega)^{-m}$ with some finite impedance value *K* and a phase modulation coefficient *m* ranging from 0 to 1. Additionally, a shunt capacitance (C_{sh}) arises from the finite capacitive coupling between the electrode lead wires and the surrounding electrolyte solution. In experiments using microwire arrays, C_{sh} is only apparent at high frequencies (>100 kHz), due to their relatively thick insulation layer. C_{sh} will have a more substantial effect when using thin film

electrodes, which have relatively thin dielectric layers and close lead spacing. These values (K, m and C_{sh}) can be experimentally determined based upon pre-implant impedance recordings in a saline buffer solution.

Typically, a spreading resistance (R_{sp}) is included in series with the CPE to describe the resistivity immediately adjacent to the electrode, but R_{sp} is nominal when compared to the rest of the model parameters and is therefore negligible (Buitenweg *et al* 1998). As the current continues to propagate toward ground *in vivo*, it would next encounter the encapsulation component. This region is composed primarily of extracellular matrix proteins and is considered to be largely resistive (Stensaas and Stensaas 1978, Edell *et al* 1992, Turner *et al* 1999, Grill and Mortimer 1994). This zone is modeled as being entirely resistive and is termed the encapsulation resistance (R_{en}).

Subsequently, the current would propagate outward from the encapsulation matrix and come across a parallel combination of a resistive extracellular matrix and neural cell membranes (Z_{tissue}). Similar to the encapsulation layer, the extracellular matrix is assumed to be principally resistive and is represented by a lumped resistance (R_{ex}). The neural cell membrane fraction of the tissue component is typified by a membrane conductance (g_m) and capacitance (C_m) scaled by the total cell membrane area (A_m). The conductance and capacitance are constant parameters drawn from the literature (Buitenweg *et al* 1998).

A simulation has been carried out to demonstrate an impedance spectrum that would be expected experimentally and its model interpretation (figure 11(D)). Model efficacy has been partially verified by colleagues interested in the application of bias voltage as a means for electrode–tissue interface rejuvenation (Johnson *et al* 2004, Johnson *et al* 2005, Otto *et al* 2006). Their results suggest that this neural impedance model may be of a predictive value based upon a correlation of an increased signal-to-noise ratio with a net decrease in model impedances.

In this model, one of the fundamental assumptions made is that the impedance of the electrodes does not change significantly over time. Alternatively, it could be proposed that the interaction of cells and tissue with the electrode surface fundamentally alters the properties of the electrode–surface interactions. In the literature, models have been proposed which suggest that the interaction between electrodes and cells could possibly affect the properties of both the electrode and the cell membrane (Grattarola and Martinoia 1993). There are observations that support the assumptions made in this study, namely that the change in the electrode impedance in saline from pre-implantation measurements to explant measurements does not change significantly compared to the changes in the impedance spectra observed during the implant duration. While this does not necessarily imply that interactions between the electrode tissue and the adjacent tissue do not alter the fundamental properties of the electrode characteristics, at this point it appears that the changes in the electrical properties of the surrounding volume of tissue contribute more significantly to the observed changes in impedance over time. This is also supported by experimental studies in culture that also suggest

that intimate cell–electrode interactions did not significantly alter electrode parameters (Buitenweg *et al* 1998). What is not understood are the long-term effects of implantation on the electrode state, since the bulk of this study involved experiments with relatively short implant durations. Further experiments and a better understanding of the mechanisms involved in electrode–tissue interactions will be useful for future electrode–tissue model development and refinement.

Conclusion

The objective of this study is to correlate the impedance properties of chronically implanted micro-electrodes with immune reactions. A series of animal experiments was conducted to characterize changes in the complex impedance of chronically implanted electrodes in neural tissue. Consistent trends in impedance changes were observed across all animals, characterized as a general increase in the measured impedance magnitude at 1 kHz that reaches a peak approximately 7 days post-implant. Histological analyses suggest that tissue reactions are confined to localized regions of the implants, around individual or groups of electrodes. Histologically described reactive responses around individual electrodes were compared to different trends in measured impedance changes. Several features of impedance changes were able to differentiate between 'confined' and 'extensive' reactive responses. In general, impedance magnitude at 1 kHz was significantly increased in extensive reactions, starting about 4 days post-implant. Electrodes with extensive reactions also displayed impedance spectra with a characteristic change at high frequencies. This change was manifested in the formation of a semi-circular arc in the Nyquist space, typical of a parallel RC network, suggestive of the infiltration of reactive cells and increased cellular density in close proximity to the electrode site. These results suggest that changes in impedance spectra are directly influenced by cellular distributions around implanted electrodes over time and that impedance measurements may provide an online assessment of cellular reactions to implanted devices.

References

Agnew W F, Yuen T G, McCreery D B and Bullara L A 1986 Histopathologic evaluation of prolonged intracortical electrical stimulation *Exp. Neurol.* **92** 162–85

Amat J A, Ishiguro H, Nakamura K and Norton W T 1996 Phenotypic diversity and kinetics of proliferating microglia and astrocytes following cortical stab wounds *Glia* **16** 368–82

Brett M A C and Brett A M O 1993 *Electrochemistry: Principles, Methods and Applications* (New York: Oxford Science)

Buitenweg J R, Rutten W L C, Willems W P A and van Nieuwkasteele J W 1998 Measurement of sealing resistance of cell-electrode interfaces in neuronal cultures using impedance spectroscopy *Med. Biol. Eng. Comput.* **36** 630–7

Burns B D, Stean J P B and Webb A C 1974 Recording for several days from single cortical neurons in completely unrestrained cats *Electroenceph. Clin. Neurophysiol.* **36** 314–8

Demirci M, Ayata C, Dalkara T, Erdemli G and Onur R 1997 Monitoring cellular edema at single-neuron level by electrical resistance measurements *J. Neurosci. Methods* **72** 175–81

Edell D J, Toi V V, McNeil V M and Clark L D 1992 Factors influencing the biocompatibility of insertable silicon microshafts in cerebral cortex *IEEE Trans. Biomed. Eng.* **39** 635–43

Ehret R, Baumann W, Brischwein M, Schwinde A, Stegbauer K and Wolf B 1997 Monitoring of cellular behavior by impedance measurements on interdigitated electrode structures *Biosensors Bioelectron.* **12** 29–41

Frampton J, Hynd M, Williams J, Shuler M and Shain W 2007 Three-dimensional hydrogel cultures for modeling changes in tissue impedance around microfabricated neural probes *J. Neural Eng.* **4** 399–409

Giaver I and Keese C R 1993 A morphological biosensor for mammalian cells *Nature* **366** 591–2

Grattarola M and Martinoia S 1993 Modeling the neuron-microtransducer junction: from extracellular to patch recording *IEEE Trans. Biomed. Eng.* **40–41** 35–41

Grill W M and Mortimer J T 1994 Electrical properties of implant encapsulation tissue *Ann. Biomed. Eng.* **22** 23–33

Johnson M D, Otto K J and Kipke D R 2005 Repeated voltage biasing improves unit recordings by reducing resistive tissue impedances *IEEE Trans. Neural. Syst. Rehabil. Eng.* **13** 160–5

Johnson M D, Otto K J, Williams J C and Kipke D R 2004 Bias voltage at microelectrodes change neural interface properties in vivo *26th Annu. Int. Conf. IEEE EMBS* (September 2004)

Jones K E, Campbell P K and Normann R A 1992 A glass/silicon composite intracortical electrode array *Annu. Biomed. Eng.* **20** 423–7

Kim Y T, Hitchcock R W, Bridge M J and Tresco P A 2004 Chronic response of adult rat brain tissue to implants anchored to the skull *Biomaterials* **25** 2229–37

Klein H C, Krop-Van Gastel W, Go K G and Korf J 1993 Prediction of specific damage or infarction from the measurement of tissue impedance following repetitive brain ischaemia in the rat *Neuropathol. Appl. Neurobiol.* **19** 57–65

Korf J, Klein H C, Venema K and Postema F 1988 Increases in striatal and hippocampal impedance and extracellular levels of amino acids by cardiac arrest in freely moving rats *J. Neurochem.* **50** 1087–96

Kyle A H, Chan C T and Minchinton A L 1999 Characterization of three-dimensional tissue cultures using electrical impedance spectroscopy *Biophys. J.* **76** 2640–8

Liu X, McCreery D B, Carter R R, Bullara L A, Yuen T G and Agnew W F 1999 Stability of the interface between neural tissue and chronically implanted intracortical microelectrodes *IEEE Trans. Rehabil. Eng.* **7** 315–26

Loda M 2000 Membranous expression of glucose transporter-1 protein (GLUT-1) in embryology neoplasms of the central nervous system *Neuropathol. Appl. Neurobiol.* **26** 91–7

Macdonald J 1992 Impedance spectroscopy *Annu. Biomed. Eng.* **20** 289–305

Maynard E M, Nordhausen C T and Normann R A 1997 The Utah intracortical electrode array: a recording structure for potential brain-computer interfaces *Electroencephalogr. Clin. Neurophysiol.* **102** 228–39

McAdams E T and Josinette J 1995 Tissue impedance: a historical overview *Physiol. Meas.* **16** A1

McAdams E T, Lackermeier A, McLaughlin, Macken D and Jossinet J 1995 The linear and non-linear electrical properties of the electrode-electrolyte interface *Biosensor Bioelectron.* **10** 67–74

McCreery D B, Yuen T G H and Bullara L A 2000 Chronic microstimulation in the feline ventral cochlear nucleus: physiological and histologic effects *Hearing Res.* **149** 223–38

Merrill D R and Tresco P A 2005 Impedance characterization of microarray recording electrodes in vitro *IEEE Trans. Biomed. Eng.* **52** 1960–6

Mooradian A D 1997 Age-related changes in glucose transporter-one mRNA structure and function *Proc. Soc. Exp. Biol. Med.* **216** 380–5

Nicolelis M A, Ghazanfar A A, Faggin B M, Votaw S and Oliveira L M 1997 Reconstructing the engram: simultaneous, multisite, many single neuron recordings *Neuron* **18** 529–37

Otto K J, Johnson M D and Kipke D R 2006 Voltage pulses change neural interface properties and improve unit recordings with chronically implanted microelectrodes *IEEE Trans. Biomed. Eng.* **53** 333–40

Polikov V S, Tresco P A and Reichert W M J 2005 Response of brain tissue to chronically implanted neural electrodes *J. Neurosci. Methods* **148** 1–18

Rousche P J and Normann R A 1998 Chronic recording capability of the Utah intracortical electrode array in cat sensory cortex *J. Neurosci. Methods* **82** 1–15

Rousche P J and Norman R A 1999 Chronic intracortical microstimulation of cat sensory cortex using the Utah intracortical electrode array *IEEE Trans. Rehabil. Eng.* **7** 56–68

Rousche P J, Pellinen D S, Pivin D P, Williams J C, Vetter R J and Kipke D R 2001 Flexible polyimide-based intracortical electrode arrays with bioactive capability *IEEE Trans. Biomed. Eng.* **48** 361–71

Schuier F J and Hossmann K A 1980 Experimental brain infarcts in cats: II. Ischemic brain edema *Stroke* **11** 593–601

Spataro L, Dilgen J, Retterer S, Spence A J, Isaacson M, Turner J N and Shain W 2005 Dexamethasone treatment reduces astroglia responses to inserted neuroprosthetic devices in rat neocortex *Exp. Neurol.* **194** 289–300

Stensaas S S and Stensaas L J 1978 Histopathological evaluation of materials implanted in the cerebral cortex *Acta Neuropathol.* **41** 145–55

Szarowski D H, Andersen M D, Retterer S C, Spence A J, Isaacson M, Craighead H G, Turner J N and Shain W 2003 Brain responses to micro-machined silicon devices *Brain Res.* **983** 23–35

Turner J N, Shain W, Szarowski D H, Andersen M, Martins S, Isaacson M and Craighead H 1999 Cerebral astrocyte response to micromachined silicon implants *Exp. Neurol.* **156** 33–49

Weiland J D and Anderson D J 2000 Chronic neural stimulation with thin-film, iridium oxide electrodes *IEEE Trans. Biomed. Eng.* **47** 911–8

Williams J C, Rennaker R L and Kipke D R 1999a Stability of chronic multichannel neural recordings: implications for a long-term interface *Neurocomputing* **26–27** 1069–76

Williams J C, Rennaker R L and Kipke D R 1999b Long-term neural recording characteristics of wire microelectrode arrays implanted in cerebral cortex *Brain Res. Protoc.* **4** 303–13

Xu J, Shepherd R K, Millard R E and Graeme M C 1997 Chronic electrical stimulation of the auditory nerve at high stimulus rates: a physiological and histopathological study *Hearing Res.* **105** 1–29